Published in final edited form as:
Nat Struct Mol Biol. 2013 August ; 20(8): 958–964. doi:10.1038/nsmb.2617.

Structurally encoded intraclass differences in EphA clusters drive distinct cell responses

Elena Seiradake[1], **Andreas Schaupp**[2], **Daniel del Toro Ruiz**[2], **Rainer Kaufmann**[1,3], **Nikolaos Mitakidis**[1], **Karl Harlos**[1], **A Radu Aricescu**[1], **Rüdiger Klein**[2], and **E Yvonne Jones**[1]

[1]Division of Structural Biology, Wellcome Trust Centre for Human Genetics, University of Oxford, Oxford, UK

[2]Max Planck Institute of Neurobiology, Martinsried, Germany

[3]Department of Biochemistry, University of Oxford, Oxford, UK

Abstract

The functional outcomes of ephrin binding to Eph receptors (Ephs) range from cell repulsion to adhesion. Here we used cell collapse and stripe assays to show contrasting effects of human ephrinA5 binding to EphA2 and EphA4. Despite equivalent ligand-binding affinities EphA4 triggered greater cell collapse, while EphA2-expressing cells adhered better to ephrinA5-coated surfaces. Chimeric receptors showed the ectodomain is a major determinant of cell response. We report crystal structures of EphA4 ectodomain alone and in complexes with ephrinB3 and ephrinA5. These revealed closed clusters with a dimeric or circular arrangement in the crystal lattice, contrasting with extended arrays previously observed for EphA2 ectodomain. Localization microscopy-based analyses showed ligand-stimulated EphA4 induces smaller clusters than EphA2. Mutant Ephs link these characteristics to interactions observed in the crystal lattices, suggesting a mechanism by which distinctive ectodomain surfaces determine clustering, and thereby signalling, properties.

Keywords

cell adhesion; cell repulsion; receptor clustering; receptor *cis* interaction; Eph–ephrin crystal structures; Eph ectodomain

The fourteen Erythropoetin-producing hepatocellular receptors (Ephs) comprise the largest family of receptor tyrosine kinases in humans. Eph receptor signalling can exert localised effects on cytoskeletal dynamics, thereby directing repulsive or migratory responses. Family

Corresponding authors: E.Y. Jones (yvonne@strubi.ox.ac.uk) R. Klein (rklein@neuro.mpg.de).

Author contributions: E. Seiradake performed protein crystallization, structure analysis, cell rounding assays and Eph clustering experiments. A. Schaupp contributed to time lapse imaging experiments. D. del Toro Ruiz performed stripe assays. R. Kaufman conducted localization microscopy data acquisition and analysis. N. Mitakidis contributed to protein crystallization. K. Harlos performed Eph crystal mounting for data collection. A.R. Aricescu, R. Klein and E.Y. Jones contributed to discussion at all stages of the project. All authors contributed to writing of the manuscript.

PDB accession codes:
EphA4 ectodomain **(**4bk4),
EphA4 ectodomain in complex with ephrinA5, methylated sample (4bk5),
EphA4 ectodomain in complex with ephrinA5 (4bka),
EphA4 ectodomain in complex with ephrinB3 (4bkf).

Author information: The authors declare no competing financial interests.

Europe PMC Funders Author Manuscripts

members are expressed in many tissues during morphogenesis, and play essential roles in cell–cell communication to guide cell positioning, segregation and migration in tissue homeostasis as well as in development[1–3]. Conversely, Ephs are widely expressed in cancer cells and in tumor blood vessels; they are implicated in tumor progression and metastatic spread, with examples of both increased and decreased levels of expression linked to malignancy[4–6].

Eph receptors bind protein ligands, the Eph receptor-interacting proteins (ephrins), presented on the surface of an opposing cell (i.e. a *trans* mode of ligand-receptor binding requiring direct cell–cell contact). All eight members of the human ephrin family are membrane-tethered, either by a glycosylphosphatidylinositol (GPI) anchor in the ephrinA proteins, or by a transmembrane helix and short cytoplasmic region in the ephrinB proteins. The Eph family is also subdivided into two classes, EphAs and EphBs; groupings that are in part determined by sequence similarity, but also reflect the general preference of EphA receptors to bind ephrinA ligands and EphB receptors to bind ephrinB ligands[7]. Within classes ephrin–Eph binding is relatively promiscuous, although measurements of binding affinities reveal some potential for selectivity in the intra-class ligand–receptor pairings[8–10].

All Eph receptors share a conserved domain composition[1] (Fig. 1a). The ectodomain comprises an N-terminal ligand-binding domain (LBD), a cysteine rich region, which can be divided into a sushi domain and an epidermal-growth-factor-like domain (EGF), followed by two fibronectin type III domains (FN1 and FN2). A single transmembrane helix connects to the intracellular tyrosine kinase domain and a sterile-alpha motif (SAM) domain that can carry a C-terminal PDZ binding motif. Likewise the ephrins are characterised by the conserved architecture of an N-terminal receptor-binding-domain (RBD). The ephrin RBD conforms to a ‘Greek key’ β barrel fold of eight β strands (designated A–K) and the Eph LBD consists of a β sandwich ‘jellyroll’ fold of twelve β strands (A–M). Structural studies of complexes between the Eph LBD and the ephrin RBD have revealed a conserved 1:1 interaction interface that is generic to all ligand-receptor combinations[10]. This high affinity binding mode is, in essence, insertion of a single long loop from the ephrin RBD (loop G–H) into a substantial cavity in the surface of the Eph LDB. The detailed architecture of this RBD–LBD interface determines the specificity and binding affinity of ephrin–Eph interactions[10]. However, the 1:1 ligand–receptor binding mode does not, in isolation, provide a molecular mechanism for Eph receptor kinase autophosphorylation and signalling. Eph signalling requires receptor clustering[11].

The first crystal structure for an Eph–ephrin complex, namely EphB2 LBD in complex with ephrinB2 RBD, highlighted a tetrameric arrangement involving a second, low affinity Eph–ephrin interaction surface. The region of the Eph LBD contributing to this interaction was designated the HI-loop[12]. Functional data[13] provided support for the biological significance of the tetrameric arrangement, however, crystallographic studies for a series of other Eph LBD–ephrin RBD complexes only revealed interfaces mediating the 1:1 high affinity binding mode[10]. Subsequent structural and functional studies on the full EphA2 ectodomain identified two in-*cis* Eph–Eph dimerisation surfaces which are equally essential for EphA2 clustering at cell–cell contacts[14,15]. These are a polar region on the LBD that includes the HI-loop plus adjacent surfaces, and a hydrophobic region on the sushi domain. Together, these interactions promote the assembly of extended EphA2 arrays that can form in the presence or absence of ephrin[14,15].

The functionality of the ephrin–Eph system is complex. Depending on receptor and ligand availability, as well as cell specific factors, Eph signalling mediates responses ranging from cell repulsion to adhesion. This variation in cellular response complicates dissection of fundamental molecular mechanisms in ephrin–Eph signalling. Eph ectodomain binding to

the receptor-binding-domain (RBD) of class A or B ephrin ligands on neighbouring cells classically triggers cell–cell repulsion through activation of the Eph intracellular kinase domain[1]. In the nervous system, repulsive EphA4–ephrin interaction is required for the formation of precise neuronal connections in the brain[16,17] and spinal cord[18], and for motor and sensory innervation of peripheral targets[19,20]. Although EphA2 protein is found in axons[21], its overall expression in the brain is low[22]. It is expressed in many other tissues[22] including the eye lens, where EphA2–ephrinA5 interaction is implicated in the adhesive packing of fibre cells through cross-talk with cadherin and catenin family proteins[23]. EphA2 is also associated with invasive cell behaviour and is up-regulated in many cancers where it increases cancer malignancy and poor clinical prognosis[4].

EphA2 only binds to class A ephrins, while EphA4 is unusually promiscuous, binding ephrinAs and Bs[7,8,24]. Both Ephs bind ephrinA5. To investigate the potential role of Eph receptor clustering characteristics in cellular response we carried out a comparative structural and functional analysis of the EphA2–ephrinA5 and EphA4–ephrinA5 systems.

RESULTS

Eph dependent differences in cellular response to ephrinA5

Whilst many factors can contribute to the functional outcome of Eph activation, we asked if Eph receptors themselves possess intrinsically distinctive properties which generate different cell responses. Cell rounding assays are widely used model systems for repulsive signalling and have been used to study Eph signalling upon stimulation with pre-clustered ephrins[25]. Cytoskeleton collapse, cell rounding, and de-adherence result from Eph kinase activation. As ligand binding affinity and kinetics could contribute to functional outcome we first sought to control for this factor. To do so we investigated the relative binding affinities of ephrinA5 to EphA2 and EphA4 in surface plasmon resonance assays. Consistent with previous ELISA-based reports[9], we found that ephrinA5 binds with similar affinity to EphA2 and EphA4 (data not shown). We engineered constructs in which full length, transmembrane, mouse EphA4 and human EphA2 receptors were fused to a fluorescent protein tag (mVenus), and expressed them in HeLa or COS7 cells (see Online Methods). Transiently transfected cells expressed EphA2 and EphA4 at comparable levels after ~20 hours (Supplementary Fig. 1). We found that EphA4-transfected cells undergo significantly stronger rounding in response to pre-clustered ephrinA5-Fc compared to EphA2-transfected cells (Fig. 1b, Supplementary Fig. 2 and Supplementary movies 1 and 2). Consistent with the low level of collapse observed with untransfected control cells, we did not detect endogenous EphA2 or EphA4 in our HeLa cell cultures (Fig. 1b and Supplementary Fig. 1). Conversely, in a stripe assay, we found that EphA2-transfected HeLa cells adhere strongly to ephrinA5-Fc coated stripes, while EphA4-transfected cells distribute more randomly between control and ephrinA5-Fc-coated stripes (Fig. 1c). What determines these Eph-specific signalling responses?

EphA4 unliganded and liganded crystal structures

To dissect the molecular properties that distinguish EphA4 ectodomain ($EphA4_{ecto}$) from EphA2 ectodomain ($EphA2_{ecto}$), we solved four crystal structures for the complete $EphA4_{ecto}$, in its unliganded form (to 3.65Å resolution), in complex with ephrinB3 RBD (1 crystal, 4.65Å) and in complex with ephrinA5 RBD (two crystals: lysine-methylated, 4.0Å, and native, 4.95Å). Data statistics, and the highest resolution shells using the $CC_{1/2}$ criteria[26] or data quality of $I/\sigma(I) > 2$ are provided in Table 1. Human $EphA4_{ecto}$ and ephrin RBD proteins were expressed in HEK293S GnTI^{-} cells, crystallized, and the structures phased by molecular replacement (see Online Methods and Supplementary Note). The unusually high solvent content of the crystals (76–88%) in conjunction with solvent

flattening methods produced good quality electron density maps despite the generally low resolution of the diffraction data sets (Table 1 and Supplementary Fig. 3). We maintained strong stereochemical restraints for refinement of the unliganded $EphA4_{ecto}$ structure and the lysine-methylated $EphA4_{ecto}$ ephrinA5 RBD complex. For the native $EphA4_{ecto}$ ephrinA5 RBD and $EphA4_{ecto}$ ephrinB3 RBD complexes we limited refinement to rigid body and TLS (Translation Libration Screw-motion) of the individual domains; stereochemical outlier residues present in high resolution molecular replacement models were not altered for these two lowest resolution structures. All four crystal structures have greater than 95% of residues in the favoured regions of the Ramachandran plot (and 0.0 – 0.4% in disallowed regions) as assessed using Molprobity[27].

The domain arrangement within $EphA4_{ecto}$ is similar to that of $EphA2_{ecto}$[14,15], with sequential LBD, sushi, EGF, FN1 and FN2 domains resulting in an oblong molecule with a ~ 90° kink at the FN1–FN2 linkage (Fig. 2a). Unlike in $EphA2_{ecto}$[14,15], the EphA4 FN1–FN2 linker conformation and relative orientation of the FN1 and FN2 domains is conserved in all four crystal structures, suggesting rigidity (Supplementary Fig. 4). The amino acid sequences of EphA2 and EphA4 in the FN1–FN2 linker region are not conserved and include a potential N-linked glycosylation site in EphA2, but not EphA4. Also, the EphA4 FN2 domain packs closely against the FN1 domain using loop residues 518–520 (Ala–Ala–Gly). Two of these residues are replaced by bulkier and more hydrophilic amino acids for the corresponding residues 512–514 in EphA2 (Gln–Glu–Gly). Taken together, these differences may underlie the reduction in inter-domain rigidity for this region in EphA2 relative to EphA4. The functional consequences of these differences in rigidity are unclear, but given the proximity of FN2 to the plasma membrane, they may impact on receptor-membrane interactions and orientation at the cell surface.

All reported structures of $EphA2_{ecto}$ revealed continuous array-like arrangements within the crystal lattice, compatible with EphA2 clustering in *cis* on the cell membrane[14,15] (Supplementary Fig. 5). Here we show that $EphA4_{ecto}$ does not form extended EphA2-like arrays in the crystal, but defined units. The $EphA4_{ecto}$ units that are compatible with in-*cis* interaction in the context of a cell surface are composed of two, three or six copies of EphA4 in a dimeric or circular arrangement (Fig. 2b). These structural data suggest that the mode of clustering observed in EphA2 cannot be extrapolated to all Eph family members. Superposition of the $EphA4_{ecto}$ structure (unliganded or bound to ephrin) on $EphA2_{ecto}$ as arranged in its characteristic arrays does not lead to obvious clashes. We conclude that surface properties, rather than differences in the overall shape, determine the mode of Eph ectodomain clustering. $EphA2_{ecto}$ arrays form through Eph–Eph interactions mediated by two specific surface patches, one centred on the HI-loop of the LBD and one on the sushi domain[14,15] (Supplementary Figs. 5 and 6). The structures reported here show that the EphA4 sushi domain can also mediate Eph–Eph interaction using the equivalent surface patch, often through dimerisation as found in $EphA2_{ecto}$ structures[14,15]. In contrast, the less conserved HI-loop region on the LBD mediates no EphA4–EphA4 contacts in three of the four $EphA4_{ecto}$ structures presented (Fig. 3 and Supplementary Figs. 6 and 7). It provides Eph–Eph contacts only in the crystal structure derived from lysine-methylated $EphA4_{ecto}$–ephrinA5 RBD complex (Supplementary Fig. 8), but as the EphA4 HI-loop contains a lysine (Fig. 3b), it may have non-native properties in this sample. Taken together, the data show that, of the two EphA2 surfaces required to build up $EphA2_{ecto}$ arrays, only one, henceforth termed the sushi dimerisation surface, is functionally conserved in EphA4 as an Eph–Eph interaction surface. The structural results further suggest that one such interaction surface is not sufficient to support the formation of EphA2-like arrays. Might Eph response to ligand be modulated by the structurally encoded clustering properties of the receptors' ectodomains?

Eph ectodomain clustering characteristics and function

To test whether differences in the clustering properties of the EphA2 and EphA4 ectodomains play a functional role in the cell, we first produced chimeras of the full length, mVenus-tagged, transmembrane receptors, in which the ectodomains of EphA2 and EphA4 were swapped (Fig. 4a). Expression levels in HeLa cells were similar to the wild type receptors (Supplementary Fig. 1). Indeed, the cell rounding assays showed the EphA4 ectodomain produced more collapse compared to EphA2 ectodomain (Fig. 4b), indicating that the Eph ectodomain is the major determinant defining the response. However, swapping the ectodomains of EphA2 and EphA4 did not fully switch the receptor functionality, suggesting that the identity of the transmembrane helix and/or the cytoplasmic region also contribute to the cell response, possibly through distinct steric or protein interaction properties in these regions. Next we sought to test whether the ectodomain-dependent functional differences relate to their clustering properties.

To directly characterize the clustering properties of fluorescently tagged EphA2 and EphA4 in COS7 cells, we used time lapse and localization microscopy techniques in living and fixed cells, respectively. Our COS7 cells expressed no EphA4 and moderate levels of endogenous EphA2 (Supplementary Fig. 1). In live cell imaging we found that EphA2 clusters formed at the cell surface within minutes after the addition of pre-clustered ephrinA5-Fc, initially with increased abundance of clusters at the cell periphery (Fig. 4c and Supplementary Fig. 9). 15-30 minutes after stimulation, EphA2 was found in large endocytic vesicles, thereby essentially clearing the cell membrane of the receptor (Supplementary Fig. 9 and data not shown). In contrast, EphA4 formed relatively small clusters and vesicles at the cell surface under the same conditions (Fig. 4c and Supplementary Fig. 9).

In order to gain quantitative information on the Eph clusters we analysed fixed cells, implementing one of the recently developed methods of super-resolution fluorescence microscopy. Spectral position determination microscopy (SPDM)[28] is a form of localization microscopy (also termed direct stochastic optical reconstruction microscopy; dSTORM[29]) that is applicable for standard fluorophores such mVenus. An intense laser excitation of the sample shifts all the fluorophores into a long-lived dark state. The stochastic recovery of individual molecules to the relatively short lived fluorescent state then separates their signals over time (and with sequential image acquisition also provides separation in space) allowing the positions of single molecules to be determined with very high accuracy. We collected data sets of individual molecular positions of mVenus-tagged wild type and chimeric Ephs in paraformaldehyde-fixed samples of COS7 cells (non-stimulated or 10 minutes post-addition of pre-clustered ephrinA5-Fc). We chose cells showing similar Eph expression levels and analysed the distribution of distances between receptor positions. To detect deviations from a spatially homogeneous distribution, i.e. clustering, we used the Ripley's L-function[30], which essentially shows the normalized distribution of distances between the single molecule positions (see Online Methods). A random distribution will approximately follow the horizontal zero-axis with constant dispersion only if the data follow a homogeneous Poisson process. Signals above zero therefore reflect both the amount of clustering (y values) and cluster diameter (x values). A further analysis of the receptor clusters was performed using a method[31] based on a threshold of local molecule density to identify and characterize individual clusters in the data sets (see Online Methods). The chimeric Eph receptors revealed that the ectodomain strongly drives the clustering properties (Fig. 4d, e and Supplementary Figs. 9 and 10). Interestingly, small clusters for EphA4 correlated with small units found in the $EphA4_{ecto}$ crystals, while larger clusters correlated with the extended arrays described for $EphA2_{ecto}$.

The molecular determinants of clustering

In order to identify whether the molecular determinants responsible for the differing functional effects were those mediating Eph–Eph interactions in the lattice assemblies of the crystal structures we designed a panel of mutant Eph-mVenus tagged constructs. EphA2^{su} and EphA4^{su} each contain the multiple mutations L254D V255D I257D in the sushi dimerisation surface. To target the EphA2 HI loop that mediates Eph–Eph contacts specifically in EphA2$_{ecto}$ crystal structures, we used the G131Y mutant EphA2^{HI}. In localization microscopy we found that mutations in the HI loop (construct EphA2^{HI}) or in the sushi dimerisation surface (construct EphA2^{su}) reduced EphA2 clustering to a level closer to that of EphA4 (Fig. 4d, e). To further validate this result we introduced a second EphA2 sushi mutant, EphA2^{su2}, containing an N-type glycosylation site in the sushi dimerization surface (H246N A248S). The bulky sugar in this region of EphA2^{su2} reduced clustering of the receptor even further compared to EphA2^{su} (Fig. 4d). EphA2^{su} had EphA4-like characteristics also in cell rounding and stripe assays (Fig. 4f). Thus targeting the array-forming abilities of EphA2 can convert its function. The equivalent mutant EphA4^{su}, also showed reduced clustering compared to wild type EphA4 (Fig. 4d). However, the overall clustering response of wild type EphA4 was low, and this further reduction was not significant.

In sequence comparisons between Ephs the sushi dimerisation surface is highly conserved, suggesting it may mediate a conserved (Eph–Eph) interaction mode across all family members, with the possible exception of EphB4 (Supplementary Fig. 11). In contrast, sequence variation in the HI-loop is high. Nevertheless, Gly131, which we show here is important in EphA2 clustering, is conserved in all EphAs except for EphA4 (Supplementary Fig. 11). It remains to be seen whether the other EphA receptors have EphA2- or EphA4-like clustering characteristics.

Ligand independent recruitment to clusters

Previously reported fluorescence microscopy data for EphA3 (ref. [32]) suggested that ephrin-independent Eph–Eph association can increase the size of clusters. To test whether the strong EphA2 clustering response observed in COS7 cells involves Eph–Eph association independently of ephrin-binding, we co-expressed in the same cell EphA2 (mCherry-tagged) and the non-ephrin-binding mutant EphA2^{nb} (mVenus-tagged). EphA2^{nb} contains mutation A190N L192S to sterically hinder high affinity ephrin binding through creation of an N-linked glycosylation site. We found, using live cell imaging, that EphA2^{nb} is recruited into clusters of stimulated wild type EphA2 (Fig. 5a). When expressed on its own, EphA2^{nb} did not cluster in response to ephrinA5-Fc addition (not shown). To find out whether the recruitment of EphA2^{nb} into EphA2 clusters depended on the array-forming Eph–Eph interaction surfaces, we co-expressed EphA2 with the non-ephrin binding mutant EphA2$^{nb\text{-}su}$, which combined the mutations in the sushi dimerisation surface (L254D V255D I257D) and in the ephrin-binding site (A190N L192S). In agreement with the crystallographic results, EphA2$^{nb\text{-}su}$ was not recruited into wild type EphA2 clusters (Fig. 5b). Supplementary Movies 3–10 show time lapse experiments of Eph clustering experiments.

DISCUSSION

The different members of the Eph receptor family are responsible for a myriad of often opposing functions including cell–cell adhesion and repulsion[1,4]. EphA4 is best known for its role as a classical guidance receptor in the neuronal system where it controls cell dynamics and motility mostly through repulsive signalling[16–19]. EphA2 has been extensively studied for its function in controlling cell adhesion, motility and invasiveness in

a variety of tissues, especially in many cancers[4]. Most previous efforts to dissect the different functionalities of Ephs have focused either on the ephrin-binding specificities[1,33] or the intracellular interactions with downstream signalling proteins[1,34]. A recent study suggested that EphA2 clustering propensities can impact on function, although the underlying mechanisms remained unclear[35]. We are now able to address this issue by structural comparison of Eph ectodomain assemblies. We found that Ephs within the same class, EphA2 and EphA4, have distinct ectodomain properties that can determine differential clustering, albeit with the caveat that a simple swap of ectodomains does not entirely switch the receptor functionality. These results demonstrate that, together with the functional contributions of the intracellular domains, the distinctive extracellular clustering characteristics can modulate signalling responses of the full length receptor. The HI-loop and its adjacent regions on the LBD harbour some of these receptor-specific features. Early structural studies using EphB2 LBD and ephrinB2 RBD implicated this region (then termed the “specificity loop”) in secondary Eph–ephrin interactions that give rise to circular Eph–ephrin hetero-tetramers[12]. The functional importance of Eph surfaces mediating hetero-tetramerisation were further confirmed in a mutagenesis study[13]. More recently, we and others presented structural data for complete EphA2 ectodomains and found that for these, the EphA2 HI-loop is part of a large homo-typic Eph–Eph interaction surface contributing to EphA2 array formation in *cis*. These results led to a new array-based model for Eph clustering[14,15]. The data reported here reveal that there is no single generic arrangement for Eph cluster formation, but rather that the different modes of interaction involving the HI-loop region reflect a diverse functional repertoire. The sushi dimerisation surface is the only surface which shows a conserved (Eph–Eph) interaction mode. In the absence of additional Eph- or ephrin-mediated interactions this surface can give rise only to dimeric, but not multimeric arrangements. It is therefore necessary, but not sufficient for array-like clustering.

Our results suggest a model in which different Eph ectodomain interaction properties are capable of dramatic modulation of signalling outputs providing an additional level of control. This model allows structural fine-tuning of functional output in cells co-expressing different Eph receptors, given their ability to form hetero-oligomeric Eph clusters[36,37], presumably through the conserved sushi dimerisation surface. The Ephs may thus exemplify a novel mechanism whereby a relatively small number of distinct receptors can control the vast number of diverse signalling processes, associated with the complexity we find in higher organisms.

EphA2 is notorious for its oncogenic effects in many cancers[4,5,35]. These effects have been, at least in part, linked to Eph kinase-independent clustering properties[38] as well as more generally to the level of the receptor–ligand clustering and activation[6]. In the results reported here we demonstrated that, by targeting surfaces involved in EphA2 clustering, we can convert EphA2 activity to resemble repulsion-mediating EphA4. The correlation of EphA2 clustering ability with breast cancer cell malignancy[35] renders this mechanism for altering cellular response therapeutically relevant. Classically, efforts in targeting Eph functions in cancers have aimed at the kinase and ligand-binding functions of the receptor, or at regulating the overall expression levels[4]. Our results highlight the potential of a perhaps more distinctive approach in which Eph receptor function can be controlled by modulation of its clustering properties.

ONLINE METHODS

Vectors and Cloning

Transmembrane constructs coding for human EphA2 (residues 27–976, Uniprot: P29317) and mouse EphA4 (residues 28–986, Uniprot Q03137) were fused to an N-terminal flag tag

(TGDYKDDDDK). Chimeric construct A2A4 was produced by fusing EphA2 ectodomain (residues 27–534) to EphA4 transmembrane and intracellular regions (residues 548–986) and an N-terminal flag tag. Chimeric construct A4A2 was produced by fusing EphA4 ectodomain (residues 28–547) to EphA2 transmembrane and intracellular regions (residues 535–976) and an N-terminal flag tag. Point mutants were generated using polymerase chain reaction techniques. All transmembrane Eph constructs were cloned into the AgeI–KpnI cloning site of a modified pHLsec vector[39] coding for an N-terminal secretion signal sequence and a C-terminal mVenus or mCherry tag followed by a polyhistidine tag. Secreted ectodomains of human EphA4 ($EphA4_{ecto}$, residues 20–547, Uniprot: P54764) and human ephrin RBDs (ephrinA5, residues 27–166, Uniprot: P52803, ephrinB3, residues 27–169, Uniprot: Q15768, ephrinB2, residues 27–167, Uniprot: P52799) were cloned into the AgeI–KpnI sites of a pHLsec vector[39] coding for an N-terminal secretion signal sequence and a C-terminal poly-His tag.

Protein purification and crystallization

We expressed $EphA4_{ecto}$, ephrinA5 RBD and ephrinB3 RBD transiently[39] in GnTI-deficient HEK293S cells[40]. Proteins were purified separately from cell culture medium using Ni-affinity and size-exclusion chromatography. Complexes were formed by mixing either before or after de-glycosylation with endoglycosidase F1 (refs. 39, 41) and subsequent lysine-methylation using established protocols[42] (see Supplementary Note). All crystals were grown at 20 °C in sitting drops using vapour diffusion[43]. Crystals of unliganded $EphA4_{ecto}$ were produced by mixing the concentrated $EphA4_{ecto}$ and ephrinB2 RBD solution (see Supplementary Note) in a 1:1 ratio (v/v) with crystallization solution 1 (1.8 M ammonium phosphate, 100 mM Hepes pH 7.4). Crystals of lysine-methylated $EphA4_{ecto}$ in complex with ephrinA5 RBD grew by mixing concentrated sample 1:1 (v/v) with crystallization solution 2 (8 % w-v Polyethylene Glycol 8000 and 0.1 M Tris-HCl pH 8.5). Native crystals of $EphA4_{ecto}$ in complex with ephrinA5 RBD grew by mixing concentrated sample 1:1:1 (v/v/v) with crystallization solution 3 (0.01 M MgSO4, 1.8 M LiSO4, 0.05 M Sodium Cacodylate pH 6) and 4% benzamidine-HCl (Hampton). Native crystals of $EphA4_{ecto}$ in complex with ephrinB3 RBD grew by mixing concentrated sample 1:1:1 (v/v/v) with crystallization solution 4 (0.08 M magnesium acetate tetrahydrate. 0.05 M cacodylate pH 6.5, 15% polyethylene glycol 400) and 0.1 M spermidine (Hampton).

Structure determinations

Diffraction data were collected at the Diamond Light Source (beam lines I24, I04, I04-1) at 100 K. Crystals were flash-frozen after brief dipping into reservoir solution supplemented with 15–25% glycerol. Diffraction data were processed using XIA2[44], XDS[45], MOSFLM[46] and CCP4 suite programs[47]. The structure of unliganded $EphA4_{ecto}$ was solved using subdomains of the previously published $EphA2_{ecto}$ model (PDB accession code 2X10)[14] as inputs for molecular replacement in PHASER[48]. The resultant model was improved using the MR_ROSETTA[49] implementation in PHENIX[50]. Electron density modification was done with PARROT[51], manual improvement of the model in COOT[52] and final rounds of refinement in autoBUSTER[53], using strong stereochemical restraints and TLS. The resultant model was used to phase the data for lysine-methylated $EphA4_{ecto}$ in complex with ephrinA5 RBD. The structure of ephrinA5 RBD, as found in complex with $EphA2_{ecto}$ (PDB accession code 2X11), was placed manually by superposition. Individual domains were refined using rigid body refinement in PHASER[50] and minor adjustments were performed by hand in COOT[52]. Electron density modification was done with PARROT[51]. A final round of refinement was done in autoBUSTER[53], using strong stereochemical restraints and TLS. The resultant model was used to phase the data for native $EphA4_{ecto}$ in complex with ephrinA5 RBD. We used the refinement program in PHENIX[50] and REFMAC5[54] for rigid body and TLS refinement of individual domains. Electron density modification was done

with PARROT[51]. The structure of $EphA4_{ecto}$ in complex with ephrinB3 RBD was solved using the model for unliganded $EphA4_{ecto}$ and the model for ephrinB3 RBD as found in complex with the Nipah virus G attachment glycoprotein (PDB accession code 3D12)[55]. Rigid body and TLS refinement were done in PHENIX[56] and BUSTER[53], electron density modification in PARROT[51].

HeLa cell collapse assay

HeLa cells were grown in life cell imaging chambers (Lab-Tek Cat. no. 155380) at 37 °C in Dulbecco's Modified Eagle's Medium (DMEM, 4.5 g/l glucose, + L-glutamine, no pyruvate, Gibco) supplemented with 1x L-glutamine (PAA), 10% foetal calf serum (HyClone) and 1x penicillin + streptomycin (PAA). Cells were transfected with Fugene or X-tremeGene HP DNA transfection reagent (Roche) following the recommended protocol and using 0.2 μg plasmid DNA per ml. After 12–15 hours, the medium was changed to imaging medium (DMEM [Cat. no. P04–05545, PAN Biotech GmbH] supplemented with 1x L-glutamine, 0.5% foetal calf serum (HyClone) and 1x penicillin + streptomycin (PAA) and the cells incubated at 37 °C for 2–6 hours. EphrinA5-Fc (R&D Cat. no. 374-EA) at 0.2 mg ml^{-1} in PBS was mixed with goat anti-human IgG Fcγ (Jackson ImmunoResearch) and imaging medium in a 5:1:28 ratio, and incubated for 2 hours at room temperature. For stimulation, the ephrinA5-Fc mixture was further diluted with pre-warmed imaging medium, and added to the cells in a final concentration of 2 μg ephrinA5-Fc + 0.04 μg anti-IgG per ml. Cells were imaged using a Zeiss Axiovert 200M microscope equipped with a temperature-controlled carbon dioxide-incubation chamber set to 37 °C, 65% humidity, 5% CO_2. Illumination was provided by an X-Cite lamp (series 120, Lumen Dynamics Group) and images were recorded by a Coolsnap HQ camera (Photometrics). Sequential images were acquired before and every 6 min following pre-clustered ephrin-Fc addition. MetaMorph imaging software (Molecular Devices) was used to analyse cell collapse responses and to assemble movies.

COS7 stimulation assay

COS7 cells were cultured, transfected and stimulated with ephrinA5-Fc + anti-human IgG as described above for HeLa cells. Cells were imaged using a confocal spinning disc microscope (Zeiss AXIO Observer Z1) and temperature-controlled incubation chamber (Zeiss) set to 37 °C, before and every 4 minutes after stimulation at 63 × magnification. 0.5 μm Z-stack slices were taken. MetaMorph imaging software was used to pick and project three in-focus Z-planes per image and to assemble movies.

Localization microscopy based analysis

COS7 cells were cultured and transfected with mVenus-tagged Eph constructs as described in previous sections. We prepared paraformaldehyde-fixed samples of non-stimulated COS7 cells, and of COS7 cells after 10 minutes of stimulation with ephrinA5-Fc + anti-IgG. Samples were mounted on regular glass slides using fluorescence mounting medium (DAKO). An OMX (optical microscope experimental, V2, API) was modified to enable localization microscopy using conventional fluorescent proteins[28]. The intensity of the 488 nm laser was adjusted to ~14 kW/cm^2 in the object plane to drive the fluorophores into a long-lived dark state, a stochastic recovery of individual molecules to the fluorescent state was recorded by image sequences of 2000 frames and an integration time of 50 ms per frame. The positions of single molecules were calculated with an estimated mean localization accuracy of < 21 nm using a Maximum-Likelihood based algorithm[57] which we adapted to the OMX hardware configuration. The resulting data sets were sorted according to their mean point densities (number of molecules recorded per μm^2). To control for the effect of Eph expression-level on clustering, only data sets with similar mean point densities (~170/μm^2) were selected for further analyses. To analyze the distances between

neighbouring molecule positions we used the Ripley's L-function[30], which takes into account distances expected for a homogenous distribution and allows interpretation of the strength of clustering (amplitude) as well as giving an indication of the size and size variance of clusters (position along the X axis, width of the distribution). Receptor clusters were identified and analysed using a previously described algorithm[31] based on a threshold value of local point density. For the present analysis the value defining what is regarded as a cluster was set to >20 molecule positions within a radius of 50 nm (~2670 points/μm^2).

Stripe assay

12.5 μg/ml of ephrinA5-Fc protein (R&D Cat. no. 374-EA) was preclustered (ratio 1:3) with Alexa594-conjugated anti-hFc antibody (Invitrogen, Cat. No. A11014) in PBS for 30 min. Clustered ephrinA5-Fc was injected into matrices (90 μm width) placed on 60 mm dishes[58], resulting in the first red-fluorescent stripes. After 30 min incubation at 37°C, dishes were washed with PBS and matrices were carefully removed. The dishes were further coated with 12.5 μg/ml of Fc (Jackson Cat. No. 009-000-008) protein pre-clustered with anti-hFc (Jackson Cat. No. 109-005-098; no fluorescent dye) for 30 min at 37°C, after that stripes were washed three times with PBS. HeLa cells, transfected with Fugene HD transfection reagent (Roche) following the manufacturer's instructions and using 0.6ug per well (6-well format), were cultured for 24 h on the stripes (30,000 cells/carpet). Cells were fixed with 4% PFA in PBS for 20 min at RT and washed with PBS. The mVenus tag in the Eph constructs was used to visualize transfected cells. Images of cells and stripes were acquired with an Axioplan epifluorescent microscope (Zeiss) at 10× magnification. Images containing stripes were further separated into two parts (on red or black stripes). The total numbers of Venus+ pixels on red stripes (ephrinA5-Fc) were quantified using Image J.

Supplementary Material

Refer to Web version on PubMed Central for supplementary material.

Acknowledgments

We thank Y. Zhao and W. Lu for protein expression, M. Jones and T.S. Walter for technical support. We are grateful to T. Gaitanos for help with confocal data acquisition, I. Davis and I.M. Dobbie for discussion and assistance at the single molecule localization facility in the Micron Advanced Bioimaging Unit, J. Erl and M. Ponserre for assistance with cell-based assays, to K.J. Morris for providing access to Metamorph software, and to R.M. Esnouf for aiding protein structure analysis. We thank the staff of the Diamond Light Source for assistance with diffraction data collection. This research was funded by a Cancer Research United Kingdom grant to E.Y.J. (grant A10979). Localization microscopy facilities in the Micron Advanced Bioimaging Unit were funded by the Wellcome Trust (grant 091911). E. Seiradake was funded by an Intra-European Fellowship (Marie Curie), D. del Toro Ruiz was funded by an European Molecular Biology Organization long-term fellowship, N. Mitakidis is supported by a Wellcome Trust D.Phil. studentship, A.R. Aricescu was supported as a United Kingdom Medical Research Council Career Development Award Fellow. Partial funding was provided by the Deutsche Forschungsgemeinschaft (SFB870) to R. Klein.

List of references for main text

1. Klein R. Eph/ephrin signalling during development. Development. 2012; 139:4105–4109. [PubMed: 23093422]
2. Batlle E, Wilkinson DG. Molecular mechanisms of cell segregation and boundary formation in development and tumorigenesis. Cold Spring Harb Perspect Biol. 2012; 4
3. Pitulescu ME, Adams RH. Eph/ephrin molecules–a hub for signaling and endocytosis. Genes Dev. 2010; 24:2480–2492. [PubMed: 21078817]
4. Pasquale EB. Eph receptors and ephrins in cancer: bidirectional signalling and beyond. Nat Rev Cancer. 2010; 10:165–180. [PubMed: 20179713]

5. Brantley–Sieders DM. Clinical relevance of Ephs and ephrins in cancer: lessons from breast, colorectal, and lung cancer profiling. Semin Cell Dev Biol. 2012; 23
6. Nievergall E, Lackmann M, Janes PW. Eph-dependent cell–cell adhesion and segregation in development and cancer. Cell Mol Life Sci. 2012; 69:1813–1842. [PubMed: 22204021]
7. Gale NW, et al. Eph receptors and ligands comprise two major specificity subclasses and are reciprocally compartmentalized during embryogenesis. Neuron. 1996; 17:9–19. [PubMed: 8755474]
8. Bowden TA, et al. Structural plasticity of eph receptor A4 facilitates cross-class ephrin signaling. Structure. 2009; 17:1386–1397. [PubMed: 19836338]
9. Noberini R, Rubio de la Torre E, Pasquale EB. Profiling Eph receptor expression in cells and tissues: a targeted mass spectrometry approach. Cell Adh Migr. 2012; 6
10. Himanen JP. Ectodomain structures of Eph receptors. Semin Cell Dev Biol. 2012; 23:35–42. [PubMed: 22044883]
11. Janes PW, Nievergall E, Lackmann M. Concepts and consequences of Eph receptor clustering. Semin Cell Dev Biol. 2012; 23:43–50. [PubMed: 22261642]
12. Himanen JP, et al. Crystal structure of an Eph receptor–ephrin complex. Nature. 2001; 414:933–938. [PubMed: 11780069]
13. Smith FM, et al. Dissecting the EphA3/Ephrin-A5 interactions using a novel functional mutagenesis screen. J Biol Chem. 2004; 279:9522–9531. [PubMed: 14660665]
14. Seiradake E, Harlos K, Sutton G, Aricescu AR, Jones EY. An extracellular steric seeding mechanism for Eph–ephrin signaling platform assembly. Nat Struct Mol Biol. 2010; 17:398–402. [PubMed: 20228801]
15. Himanen JP, et al. Architecture of Eph receptor clusters. Proc Natl Acad Sci U S A. 2010; 107:10860–10865. [PubMed: 20505120]
16. Egea J, et al. Regulation of EphA 4 kinase activity is required for a subset of axon guidance decisions suggesting a key role for receptor clustering in Eph function. Neuron. 2005; 47:515–528. [PubMed: 16102535]
17. Dufour A, et al. Area specificity and topography of thalamocortical projections are controlled by ephrin/Eph genes. Neuron. 2003; 39:453–465. [PubMed: 12895420]
18. Kullander K, et al. Role of EphA4 and EphrinB3 in local neuronal circuits that control walking. Science. 2003; 299:1889–1892. [PubMed: 12649481]
19. Kao TJ, Law C, Kania A. Eph and ephrin signaling: lessons learned from spinal motor neurons. Semin Cell Dev Biol. 2012; 23
20. Wang L, Klein R, Zheng B, Marquardt T. Anatomical coupling of sensory and motor nerve trajectory via axon tracking. Neuron. 2011; 71
21. Brittis PA, Lu Q, Flanagan JG. Axonal protein synthesis provides a mechanism for localized regulation at an intermediate target. Cell. 2002; 110:223–235. [PubMed: 12150930]
22. Hafner C, et al. Differential gene expression of Eph receptors and ephrins in benign human tissues and cancers. Clin Chem. 2004; 50:490–499. [PubMed: 14726470]
23. Cooper MA, et al. Loss of ephrin-A5 function disrupts lens fiber cell packing and leads to cataract. Proc Natl Acad Sci U S A. 2008; 105:16620–16625. [PubMed: 18948590]
24. Qin H, et al. Structural characterization of the EphA4–Ephrin-B2 complex reveals new features enabling Eph–ephrin binding promiscuity. J Biol Chem. 2010; 285:644–654. [PubMed: 19875447]
25. Poliakov A, Cotrina M, Wilkinson DG. Diverse roles of eph receptors and ephrins in the regulation of cell migration and tissue assembly. Dev Cell. 2004; 7:465–480. [PubMed: 15469835]
26. Karplus PA, Diederichs K. Linking crystallographic model and data quality. Science. 2012; 336:1030–1033. [PubMed: 22628654]
27. Davis IW, et al. MolProbity: all-atom contacts and structure validation for proteins and nucleic acids. Nucleic Acids Res. 2007; 35:W375–383. [PubMed: 17452350]
28. Lemmer P, et al. SPDM: light microscopy with single-molecule resolution at the nanoscale. Applied Physics B. 2008; 93:1–12.
29. Heilemann M, et al. Subdiffraction-resolution fluorescence imaging with conventional fluorescent probes. Angew Chem Int Ed Engl. 2008; 47:6172–6176. [PubMed: 18646237]
30. Ripley BD. Modeling Spatial Patterns. J Roy Stat Soc B Met. 1977; 39:172–212.

31. Kaufmann R, Mueller P, Hildenbrand G, Hausmann M, Cremer C. Analysis of Her2/neu membrane protein clusters in different types of breast cancer cells using localization microscopy. J Microsc. 2011; 242:46–54. [PubMed: 21118230]
32. Wimmer-Kleikamp SH, Janes PW, Squire A, Bastiaens PI, Lackmann M. Recruitment of Eph receptors into signaling clusters does not require ephrin contact. J Cell Biol. 2004; 164:661–666. [PubMed: 14993233]
33. Triplett JW, Feldheim DA. Eph and ephrin signaling in the formation of topographic maps. Semin Cell Dev Biol. 2012; 23:7–15. [PubMed: 22044886]
34. Astin JW, et al. Competition amongst Eph receptors regulates contact inhibition of locomotion and invasiveness in prostate cancer cells. Nat Cell Biol. 2010; 12:1194–1204. [PubMed: 21076414]
35. Salaita K, et al. Restriction of receptor movement alters cellular response: physical force sensing by EphA2. Science. 2010; 327:1380–1385. [PubMed: 20223987]
36. Janes PW, et al. Eph receptor function is modulated by heterooligomerization of A and B type Eph receptors. J Cell Biol. 2011; 195:1033–1045. [PubMed: 22144690]
37. Freywald A, Sharfe N, Roifman CM. The kinase-null EphB6 receptor undergoes transphosphorylation in a complex with EphB1. J Biol Chem. 2002; 277:3823–3828. [PubMed: 11713248]
38. Miao H, et al. EphA2 mediates ligand-dependent inhibition and ligand-independent promotion of cell migration and invasion via a reciprocal regulatory loop with Akt. Cancer Cell. 2009; 16:9–20. [PubMed: 19573808]

Methods-only references

39. Aricescu AR, Lu W, Jones EY. A time- and cost-efficient system for high-level protein production in mammalian cells. Acta Crystallogr D Biol Crystallogr. 2006; 62:1243–1250. [PubMed: 17001101]
40. Reeves PJ, Callewaert N, Contreras R, Khorana HG. Structure and function in rhodopsin: high-level expression of rhodopsin with restricted and homogeneous N-glycosylation by a tetracycline-inducible N-acetylglucosaminyltransferase I-negative HEK293S stable mammalian cell line. Proc Natl Acad Sci U S A. 2002; 99:13419–13424. [PubMed: 12370423]
41. Grueninger-Leitch F, D'Arcy A, D'Arcy B, Chene C. Deglycosylation of proteins for crystallization using recombinant fusion protein glycosidases. Protein Sci. 1996; 5:2617–2622. [PubMed: 8976570]
42. Walter TS, et al. Lysine methylation as a routine rescue strategy for protein crystallization. Structure. 2006; 14:1617–1622. [PubMed: 17098187]
43. Walter TS, et al. A procedure for setting up high-throughput nanolitre crystallization experiments. Crystallization workflow for initial screening, automated storage, imaging and optimization. Acta Crystallogr D Biol Crystallogr. 2005; 61:651–657. [PubMed: 15930615]
44. Winter G. xia2: an expert system for macromolecular crystallography data reduction. Journal of Applied Crystallography. 2010; 43:186–190.
45. Kabsch W. Automatic processing of rotation diffraction data from crystals of initially unknown symmetry and cell constants. Journal of Applied Crystallography. 1993; 26:795–800.
46. Leslie AG. The integration of macromolecular diffraction data. Acta Crystallogr D Biol Crystallogr. 2006; 62:48–57. [PubMed: 16369093]
47. Collaborative Computational Project 4. The CCP4 suite: programs for protein crystallography. Acta Crystallogr D Biol Crystallogr. 1994; 50:760–763. [PubMed: 15299374]
48. McCoy AJ, et al. Phaser crystallographic software. Journal of Applied Crystallography. 2007; 40:658–674. [PubMed: 19461840]
49. DiMaio F, Tyka MD, Baker ML, Chiu W, Baker D. Refinement of protein structures into low-resolution density maps using rosetta. J Mol Biol. 2009; 392:181–190. [PubMed: 19596339]
50. Zwart PH, et al. Automated structure solution with the PHENIX suite. Methods Mol Biol. 2008; 426:419–435. [PubMed: 18542881]
51. Zhang KY, Cowtan K, Main P. Combining constraints for electron-density modification. Methods Enzymol. 1997; 277:53–64. [PubMed: 18488305]

52. Emsley P, Cowtan K. Coot: model-building tools for molecular graphics. Acta Crystallogr D Biol Crystallogr. 2004; 60:2126–2132. [PubMed: 15572765]

53. Blanc E, et al. Refinement of severely incomplete structures with maximum likelihood in BUSTER-TNT. Acta Crystallogr D Biol Crystallogr. 2004; 60:2210–2221. [PubMed: 15572774]

54. Murshudov GN, Vagin AA, Dodson EJ. Refinement of macromolecular structures by the maximum-likelihood method. Acta Crystallogr D Biol Crystallogr. 1997; 53:240–255. [PubMed: 15299926]

55. Xu K, et al. Host cell recognition by the henipaviruses: crystal structures of the Nipah G attachment glycoprotein and its complex with ephrin-B3. Proc Natl Acad Sci U S A. 2008; 105:9953–9958. [PubMed: 18632560]

56. Adams PD, et al. PHENIX: building new software for automated crystallographic structure determination. Acta Crystallogr D Biol Crystallogr. 2002; 58:1948–1954. [PubMed: 12393927]

57. Gruell, F.; Kirchgessner, M.; Kaufmann, R.; Hausmann, M.; Kebschull, U. International Conference on Field Programmable Logic and Applications; IEEE; 2011.

58. Knoll B, Weinl C, Nordheim A, Bonhoeffer F. Stripe assay to examine axonal guidance and cell migration. Nat Protoc. 2007; 2:1216–1224. [PubMed: 17546017]

Europe PMC Funders Author Manuscripts

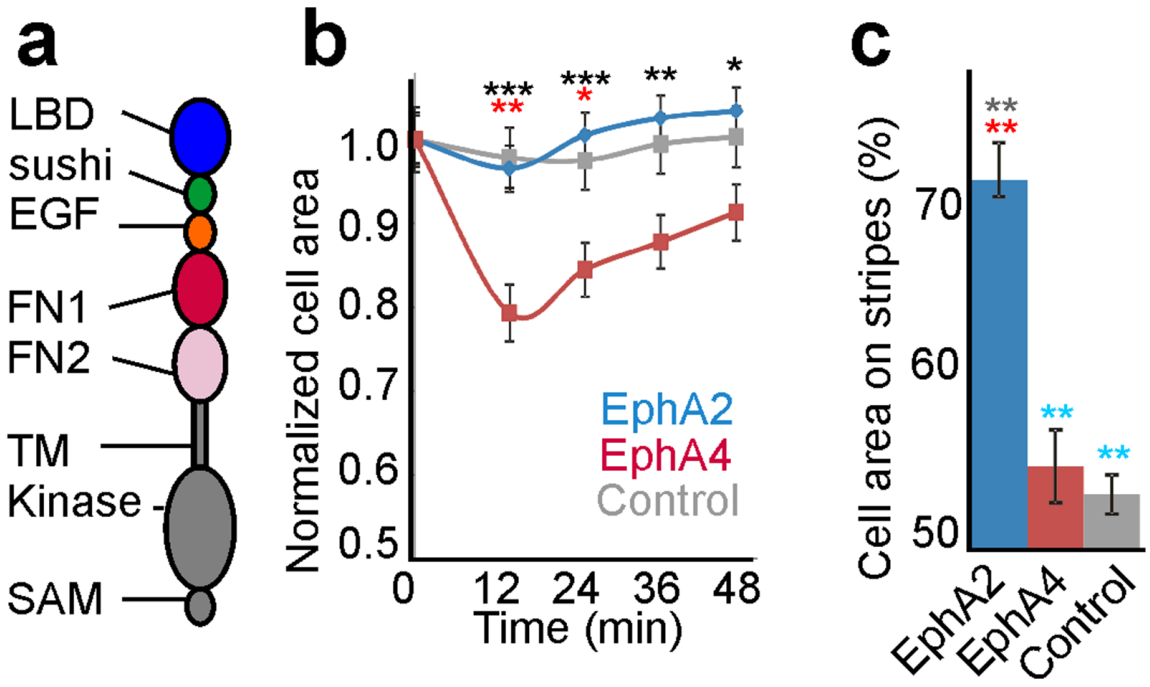

Fig. 1. Stimulation of EphA2 and EphA4 trigger different cell responses.

a) Schematic overview showing Eph domain composition: ligand-binding domain (LBD), sushi, epidermal-growth-factor-like (EGF), fibronectin type III (FN1 and FN2), transmembrane helix (TM), tyrosine kinase and sterile-alpha motif (SAM). Domains are coloured separately for the ectodomain.

b) Rounding responses of non-transfected control and Eph-transfected HeLa cells upon ephrinA5-Fc stimulation were measured. Average adherent cell surface areas were normalized using the values at time =0 (before receptor stimulation). Statistical significance was determined using one-way ANOVA and Tukey's post hoc test and is shown with red stars (control, EphA4) and black stars (EphA2, EphA4). Error bars denote s.e.m. **P* < 0.05, ***P* < 0.01, ****P* < 0.001.

c) Hela cell stripe assay. Adhesion of Eph-transfected cells to ephrinA5-Fc coated surfaces is shown (50% corresponds to random distribution, > 50% reflects adhesion). Statistical significance was calculated with one-way ANOVA and Tukey's post hoc test and is shown with red stars (to EphA4), blue stars (to EphA2) and grey stars (to control). Error bars denote s.e.m. ***P* < 0.01.

Europe PMC Funders Author Manuscripts

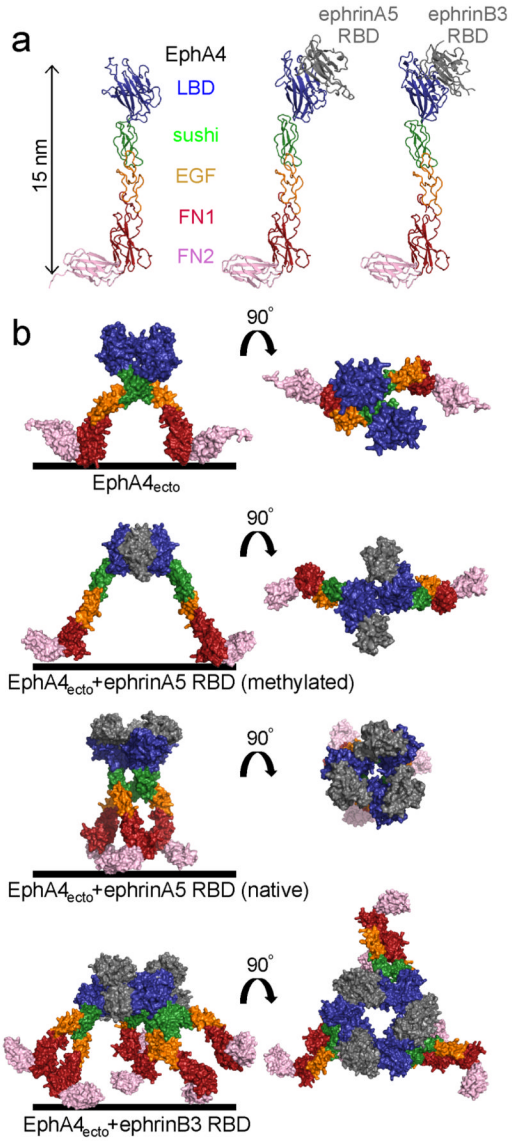

Fig. 2. EphA4 ectodomain forms oligomeric units in crystal lattices.

a) Cartoon diagrams are shown of complete EphA4 ectodomain ($EphA4_{ecto}$), unliganded or in complex with ephrinA5 or ephrinB3 receptor-binding domain (RBD). EphA2 domains are coloured separately as indicated. Ligand-binding domain (LBD), epidermal-growth-factor-like (EGF), fibronectin type III domains 1 and 2 (FN1 and FN2). Ephrins are coloured in grey.

b) Crystal lattice assemblies that are compatible with clustering of receptors on the same cell (in *cis*) are shown as surface representations for the four crystal structures presented (side and top views). Colours are as in panel a.

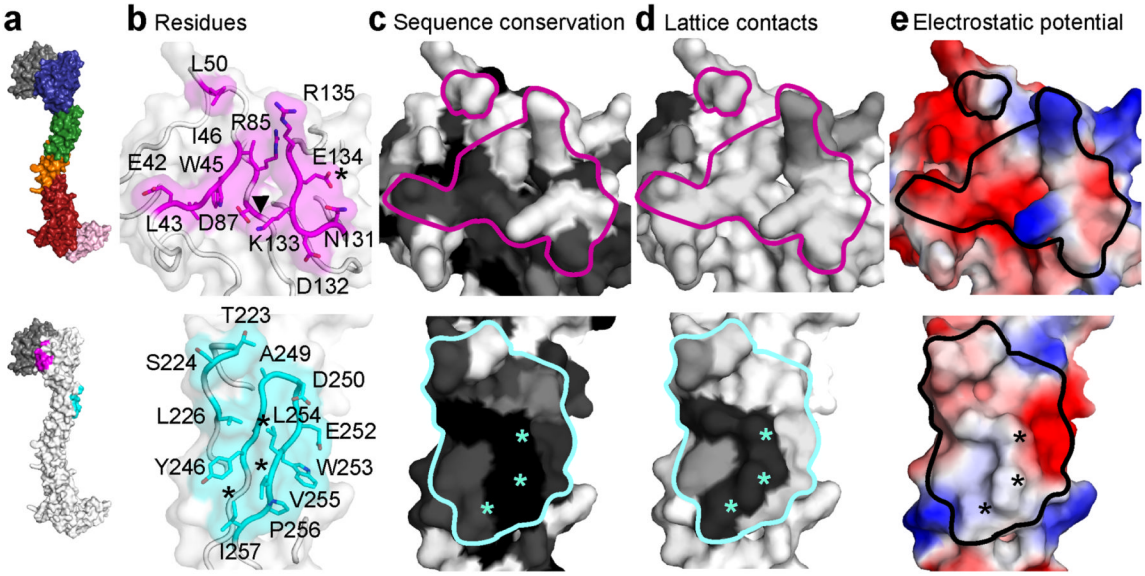

Fig. 3. Properties of the EphA4 HI-loop area and sushi dimerization region.

a) The surface of $EphA4_{ecto}$ in complex with ephrinB3 RBD is shown in two colour schemes. Top: domains are coloured separately as in Fig. 2. Bottom: colours are white (EphA4), grey (ephrinB3), magenta (HI-loop and adjacent regions implicated in clustering for EphA2 (ref. [14])) and cyan (sushi dimerization surface).

b–e) Zoomed-in view of the EphA4 HI-loop region (magenta) and sushi dimerization surfaces (cyan). **b)** Residues are shown as sticks. Lys133 is marked with an arrow. An asterisk marks Glu134, equivalent to Gly131 in EphA2, which is mutated to tyrosine in $EphA2^{HI}$. Three asterisks mark the surface residues Leu254, Val255 and Ile257 on the sushi domain. These are mutated to aspartate in $EphA4^{su}$, $EphA2^{su}$ and $EphA2^{nb\text{-}su}$.

c) Colours are according to sequence conservation among human EphAs (ranging from black = highly conserved, to white = not conserved). The HI-loop area and sushi dimerization surface are encircled.

d) Colours are according to the frequency of residues mediating lattice contacts in the four crystal structures presented (ranging from black = involved in all lattices, to white = not involved in any lattices).

e) Colours are according to electrostatic potential, calculated for vacuum (ranging from blue = positive charge, to red = negative charge, units in Pymol (DeLano, W. L.) adjusted to +/−63 . White = neutral).

Europe PMC Funders Author Manuscripts

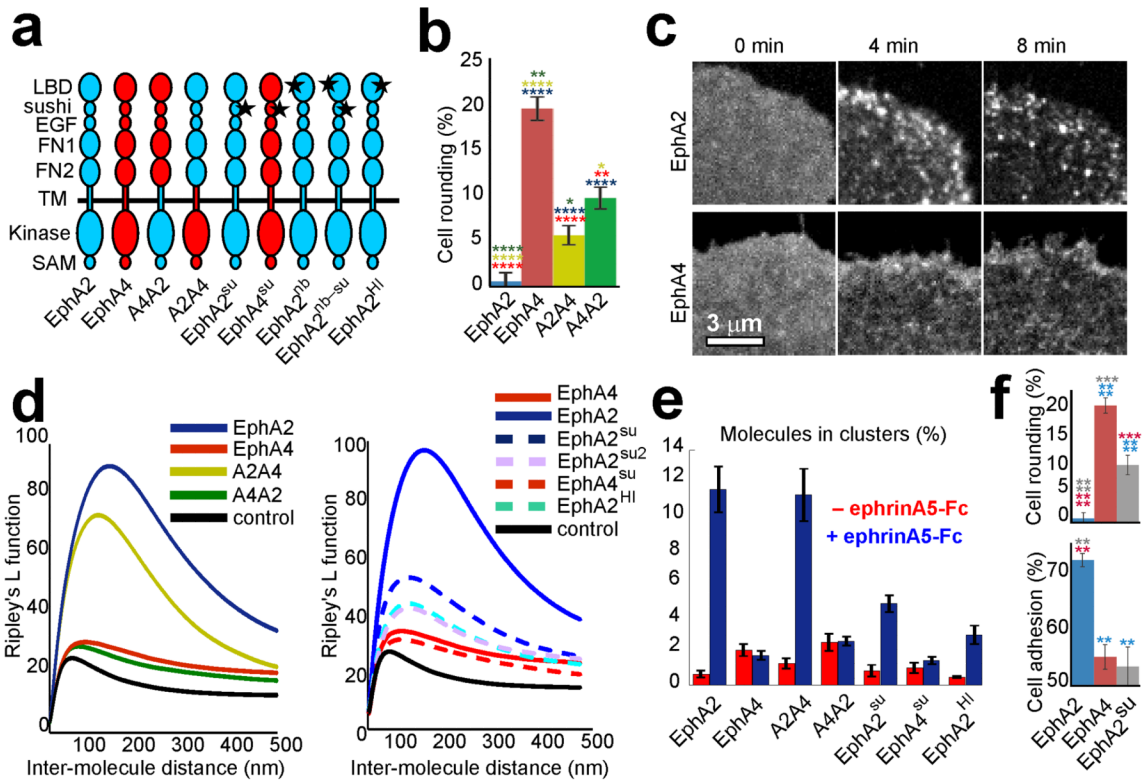

Fig. 4. Eph ectodomains can control Eph clustering and function.

a) Schematic representation of transmembrane Eph constructs: EphA2 blue, EphA4 red. Chimeric proteins were engineered by swapping ectodomains (A2A4 or A4A2). Stars mark point mutants in the HI-loop, sushi dimerization and major ephrin-binding sites. All constructs contain an N-terminal Flag tag and a C-terminal mVenus or mCherry tag.

b) HeLa cell rounding responses measured 10 minutes after ephrinA5-Fc stimulation. Plotted are averaged ratios of the adherent cell surface after and before stimulation. Statistical significance to EphA2 and EphA4 samples (one-way ANOVA and Tukey's post hoc test) is shown with blue and red stars, respectively. A two-tailed T-test was used to calculate significance between A2A4 and A4A2. Error bars denote s.e.m. **P* < 0.05, ***P* < 0.01, *****P* < 0.0001.

c) Confocal time lapse images. Eph clustering was induced by ephrinA5-Fc stimulation in COS7 cells.

d) Single molecule experiments were performed using localization microscopy. Normalized Ripley's L functions (L(r)-r)) are plotted over the distances (r(nm)) between the molecules. Increased (L(r)-r)) at particular distances reflect the amount of clustering and the cluster sizes.

e) Further quantification of data presented in panel d. The percentage of detected molecules present in clusters is shown. Clusters were defined as molecules having at least 20 neighbouring molecules within a radius of 50 nm (Supplementary Fig. 10).

f) Cell rounding in response to pre-clustered ephrinA5-Fc and cell adhesion to ephrinA5-Fc containing stripes was measured using transfected HeLa cells. EphA2 blue, EphA4 red, EphA2^{su} grey. Statistical significance was determined using one-way ANOVA and Tukey's post hoc test. Error bars denote s.e.m. ***P* < 0.01, ****P* < 0.001, *****P* < 0.0001.

Europe PMC Funders Author Manuscripts

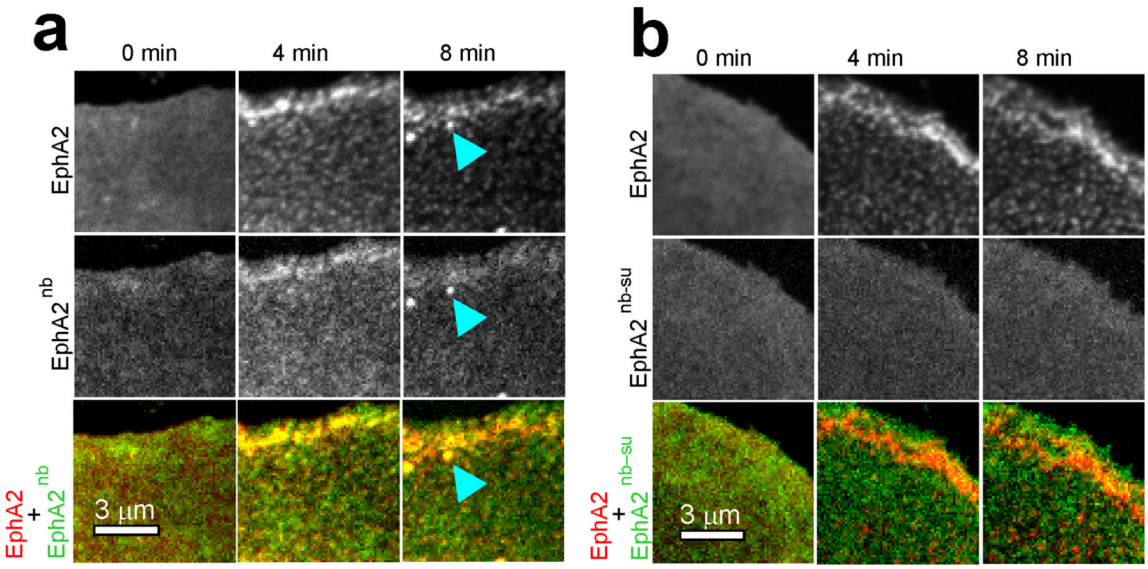

Fig. 5. Non-ligand-bound EphA2 clustering depends on Eph–Eph ectodomain interactions.

a) Live COS7 cell time lapse experiment showing co-clustering of the non-ephrin binding mutant EphA2^{nb}-mVenus with EphA2-mCherry. Blue arrows indicate a co-clustering event. **b)** As in panel a, but using a non-ephrin-binding mutant EphA2$^{nb\text{-}su}$-mVenus with mutations in the sushi dimerization surface.

Europe PMC Funders Author Manuscripts

Table 1

	EphA4 ectodomain	EphA4 ectodomain + ephrinA5 (methylated)	EphA4 ectodomain + ephrinA5 (not methylated)	EphA4 ectodomain + ephrinB3
Data collection				
Space group	*P3221*	*H32*	*H32*	*P4332*
Cell dimensions				
a, *b*, *c* (Å)	166.88, 166.88, 192.07	256.95 256.95 252.51	202.88 202.88 326.51	300.53 300.53 300.53
Resolution (Å)[a]	83–3.65 (3.7–3.65)	70–4.0 (4.05–4.00)	48–4.95 (5.00–4.95)	106–4.65 (4.7–4.65)
R_{meas} (%)[a,b]	19.2 (545)	41.0 (586)	74.3 (558)	26.2 (367)
$CC_{1/2}$[b]	100 (17.7)	99.7 (15.9)	95.8 (22.0)	99.9 (16.1)
$I / \sigma(I)$[a]	14.17 (0.48)	7.74 (0.59)	3.32 (0.32)	7.7 (0.50)
Highest resolution shell with $I/\sigma(I)$ >2 (Å)	4.2–4.1	4.55–4.45	7.0–6.9	5.8–5.7
Completeness (%)[a]	99.9 (100)	99.9 (100)	99.7 (98.5)	99.9 (99.9)
Redundancy[a]	20.0 (20.1)	11.3 (11.3)	9.4 (7.6)	10.8 (6.9)
Refinement				
Resolution (Å)[a]	48.2–3.65 (3.76–3.65)	70–4.0 (4.15–4.0)	48–4.95 (5.08–4.95)	106–4.65 (4.84–4.65)
No. reflections[a]	34842 (2951)	27150 (2680)	11147 (744)	25492 (2802)
R_{work} / R_{free}	0.349 / 0.386	0.313 / 0.321	0.396 / 0.414	0.328 / 0.342
No. atoms (all protein)	6344	5087	5087	10126
average *B*-factor	125.0	188.0	243.0	221.2
R.m.s. deviations				
Bond lengths (Å)	0.007	0.007	0.007	0.010
Bond angles (°)	0.85	0.87	0.87	1.01

[a] Values in parentheses are for highest-resolution shell.

[b] Criteria for data cutoff were from ref. 26.